

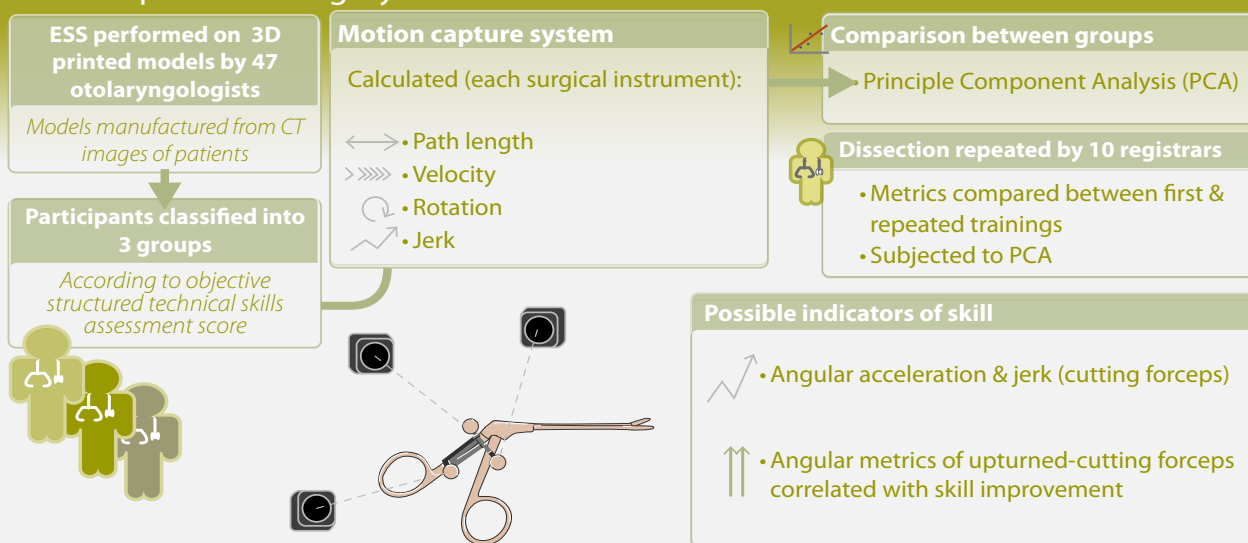
Motion analysis for objective evaluation of psychomotor skills in Endoscopic Sinus Surgery

Kou Miyaji^{1, #}, Masanobu Suzuki^{2, #}, Ryosuke Watanabe², Takayoshi Suzuki², Kotaro Matoba³, Akira Nakazono², Yuji Nakamaru², Koki Ebina¹, Takashige Abe⁴, Dominik Hinder⁵, A.J. Psaltis⁵, P.J. Wormald¹, Akihiro Homma², Atsushi Konno¹

Rhinology 63: 2, 190 - 199, 2025

<https://doi.org/10.4193/Rhin22.320>

Motion analysis for objective evaluation of psychomotor skills in Endoscopic Sinus Surgery



Combined with 3D-printed sinus models, motion capture provided objective evaluation of surgical performance in ESS

Miyaji K, Suzuki M, Watanabe R, et al. Rhinology 2025. <https://doi.org/10.4193/Rhin22.320>

RHINOLOGY
Official Journal of the European and American Societies

Abstract

Background: This study aims to digitalize surgical maneuvers in ESS using a motion capture system under standardized conditions provided by 3D printed-sinus models. **Methodology:** Forty-seven otolaryngologists performed ESS on 3D printed models manufactured from computed tomography (CT) images of actual patients. Participants were classified to 3 groups according to the objective structured technical skills assessment score. All surgical maneuvers performed during ESS were captured by a motion capture system. The path length, velocity, acceleration, and jerk were calculated for each surgical instrument and compared among the groups. Principle Component Analysis (PCA) was utilized to identify which metrics reflected surgical skill level. In addition, ten registrars repeated the surgical dissection. Their motion metrics were also compared between first training and the repeated training and then subjected to the PCA. **Results:** Several metrics such as the angular acceleration and jerk of the cutting forceps were identified by PCA as possible indicators distinguishing the different skill levels for the ESS maneuvers. PCA analysis in the repetitive training also found the angular metrics of the upturned-cutting forceps correlating to their skill improvement. **Conclusions:** Combined with the validated 3D-printed sinus models, the motion capture system provided the objective evaluation of the surgical performances of ESS.

Key words: motion capture, surgical education, 3D-printer, simulation training, off-the-job training

Introduction

Endoscopic Sinus Surgery (ESS) is the standard surgical procedure for the management of chronic rhinosinusitis ⁽¹⁾. ESS requires a unique set of surgical skills. It requires a two-handed fine manipulation of endoscopes and instruments to create a non-intuitive endoscopic 2D views on which surgical steps are performed. The anatomical proximity to the orbits and skull base creates significant associated risks with the surgery. Therefore, in order to perform safe and effective surgery, surgeons need specific training in ESS techniques ⁽²⁾.

Several factors have increased the demand for surgical training including work hour restrictions in residency programs and ethical concerns about patients' safety in so-called "on-the-job training". In addition, there has been increased interest in the standardization of the evaluation of surgeons undertaking exit examinations with objective assessment of surgical skill deemed a necessary part of the qualification process in addition to theoretical knowledge. One of factors that have restricted the evaluation of endoscopic sinus surgical skill is the significant diversity of the anatomy of paranasal sinuses and the lack of methods to analyze the fine motor skill and dexterity of the surgeon. A recent publication by our group showed validated the use of 3D-printed sinus models as a teaching medium for ESS surgical performance, with sufficient face, content, and concurrent validity ⁽³⁾.

A recent proposed solution to the evaluation of these surgical skills is the motion capture system. Motion capture is the process of tracking and digitalizing the movements of objects in space. The systems include optical, inertial sensors, mechanical, and magnetic systems. In the optical system, infrared reflective markers are attached to people or objects, and two or more cameras track the markers. The 3D position of the marker is localized by combining the 2D position of the marker on each camera image, of which the positional relationship had been identified in the calibration process prior to measurements. The position (x, y, z) and orientation (roll, pitch, yaw) of a rigid body can be localized by attaching three or more markers to the rigid body. The acquired data also can be visualized in computed graphic images in real time. Such digitalization allows for objective evaluation of the motion. The usefulness of the system has been reported in a variety of medical procedures, including laparoscopy ⁽⁴⁻⁹⁾, arthroscopy ⁽¹⁰⁾, bipolar hemostasis ⁽¹¹⁾, transcatheter aortic valve implantation ⁽¹²⁾, central venous access procedure ⁽¹³⁾, obstetric ultrasound echoes ⁽¹⁴⁾ and tracheal intubation ⁽¹⁵⁾. To date there have been no reports applying the motion capture system to ESS. There are, however, several challenges with ESS as the surgical field is constricted and there is simultaneous use of an endoscope and multiple surgical instruments all with access through one nostril.

In this study, we examined the feasibility of the objective evaluation of ESS surgical performance by a newly designed motion

capture system and manufactured 3D-printed sinus models. We also tried to identify the motion metrics reflecting the different levels of surgical skills, aiming for objective evaluation of the surgical skills in the future.

Materials and methods

Participants

This study was performed concurrently with the previously published study on the validation of surgical training using 3D sinus models ⁽³⁾. Forty-seven otolaryngologists voluntarily participated in the study. Before the study was performed, the purpose and design of the study was explained to the participants. The written informed consent was obtained from all participants.

Mock surgeries

The participants performed ESS surgeries on 3D-printed models in a sitting position, as previously reported ⁽³⁾. Briefly, a 4-mm rigid nasal endoscope and a monitor (Telepac, Storz, Tuttlingen, Germany), standard ESS instruments (Storz), a powered microdebrider (Medtronic, Jacksonville, FL, USA) and 3D-printed models (Fusetec, Adelaide, South Australia) were prepared. The models were manufactured using 3D-printer technology from the CT scans of actual patients with chronic rhinosinusitis and validated for ESS training ⁽³⁾. Infrared reflective markers were attached to the endoscope, pediatric backbiter forceps, straight-cutting forceps, and upturned-cutting forceps, and the basement for 3D printed models. The infrared reflective markers had individual arrangement patterns so that the motion capture system could recognize and identify multiple instruments simultaneously. The participants were allocated 45 minutes to complete a full house ESS (sphenoidectomy with frontal sinusotomy and maxillary antrostomy). Their surgical performances were assessed by an expert rhinologist (MS) according to the Objective Structured Assessment of Technical Skills (OSATS) score for ESS ⁽¹⁶⁾. The interrater reliability of the OSATS score in this study was confirmed to be sufficiently high ($r=0.957$, $p<0.001$) in the previous report ⁽³⁾. The assessment was done independently of surgical experience. Participants were classified to three groups according to their OSATS scores (experts: the top 1/3, intermediates: the middle 1/3, and novices: the bottom 1/3 of the scores; Figure 1). After the surgeries, a questionnaire survey was done to evaluate how much the installed markers interfered with the procedure.

First, all participants performed the surgeries for Model 2 Right side (Figure 1A). The motion metrics were analyzed as described below, and compared among the experts, the intermediates, and the novices. Further, ten otolaryngology registrars (ENT surgical trainees) among the participants performed the surgeries an additional six times as repetitive training. In the 1st and

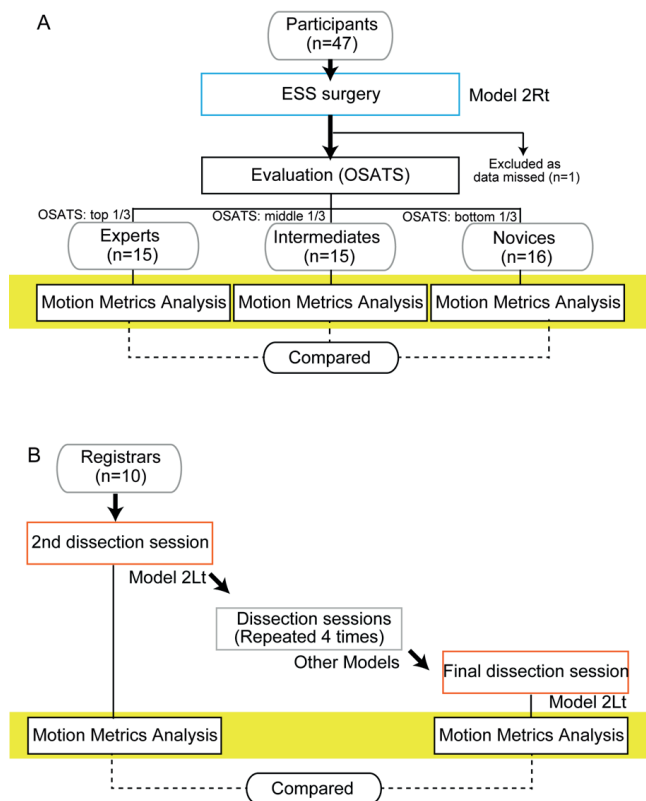


Figure 1. The flow of the present study. (A) Forty-seven participants performed ESS mock surgeries on 3D-printed models (Model 2Rt). Participants were classified to three groups according to the Objective Structured Assessment of Technical Skills (OSATS) score for ESS (experts: the top 1/3, intermediates: the middle 1/3, and novices: the bottom 1/3 of the scores). The motion metrics were analyzed and compared among the experts, the intermediates, and the novices. (B) Ten otolaryngology registrars performed the mock surgeries an additional six times as repetitive training. In the 1st and the final training (2nd, and 7th surgeries in total, respectively), Model 2Lt were used to compare their motion metrics.

the final training (2nd, and 7th surgeries in total, respectively), Model 2 Left were used to compare their motion metrics (Figure 1B). More details of the models and the repetitive training were previously described⁽³⁾.

Motion analysis

To measure the ESS hand maneuver, a newly developed optical motion capture system was utilized^(4,17). During the surgeries, 11 infrared cameras (OptiTrack Prime 41, NaturalPoint Inc., Corvallis, OR, USA) tracked the infrared reflective markers attached to the 3D model, the endoscope, and the forceps, at 100 frame per second (Figure 2, Figure S1, and supplementary video). The deficient ratio was determined as the percent of the time that motion metrics were not captured. The endoscope and each forceps had four infrared reflective markers with individual arrangement patterns, respectively, so that the motion capture system could

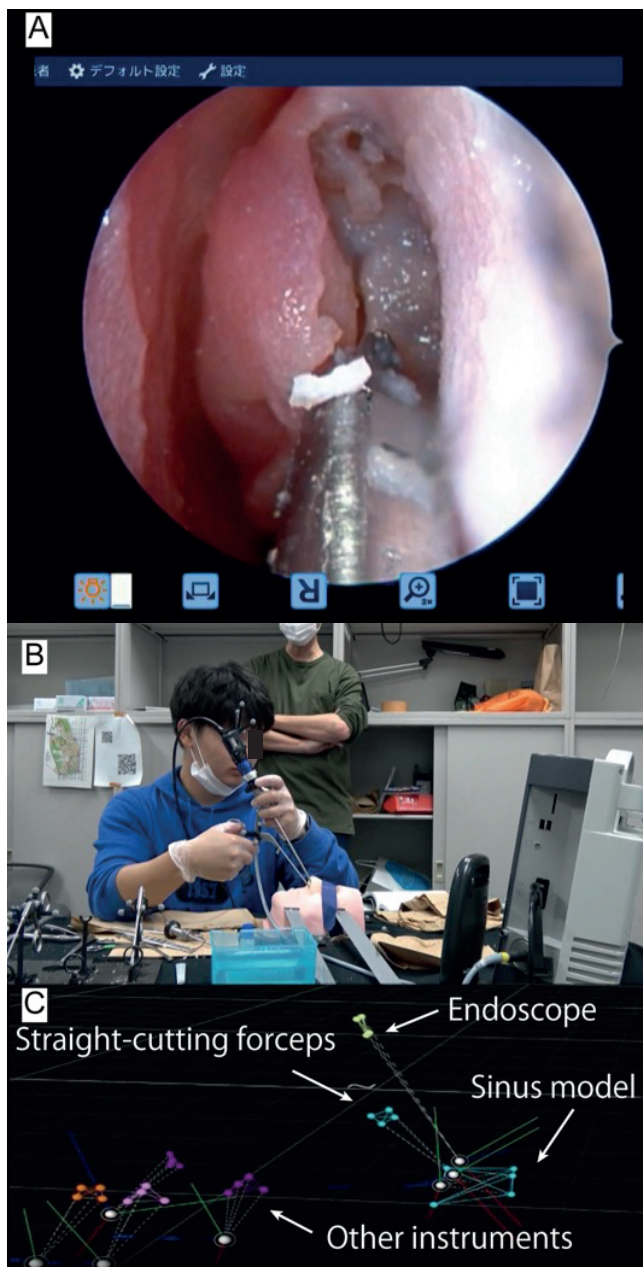


Figure 2 and Video S1. Overview of the measurement system of hand maneuver for ESS. (A) The endoscopic view of the mock surgery for the 3D models. (B) A participant engaging in the mock surgery. The infrared reflective markers attached to the surgical instruments were tracked with 11 infrared cameras. (C) Computer display showing the movements of surgical instruments. Sky-blue and yellow dots corresponding to the reflective markers attached to the pediatric backbiter forceps and the endoscopy, respectively.

localize the position (x, y, z) and orientation (roll, pitch, yaw) of multiple instruments simultaneously. The tip position of the instruments was calculated from the position and orientation of the marker set attached to the handle of the instrument. The motion of the surgical instruments was analyzed in two coordinate systems: the Cartesian coordinate system and the

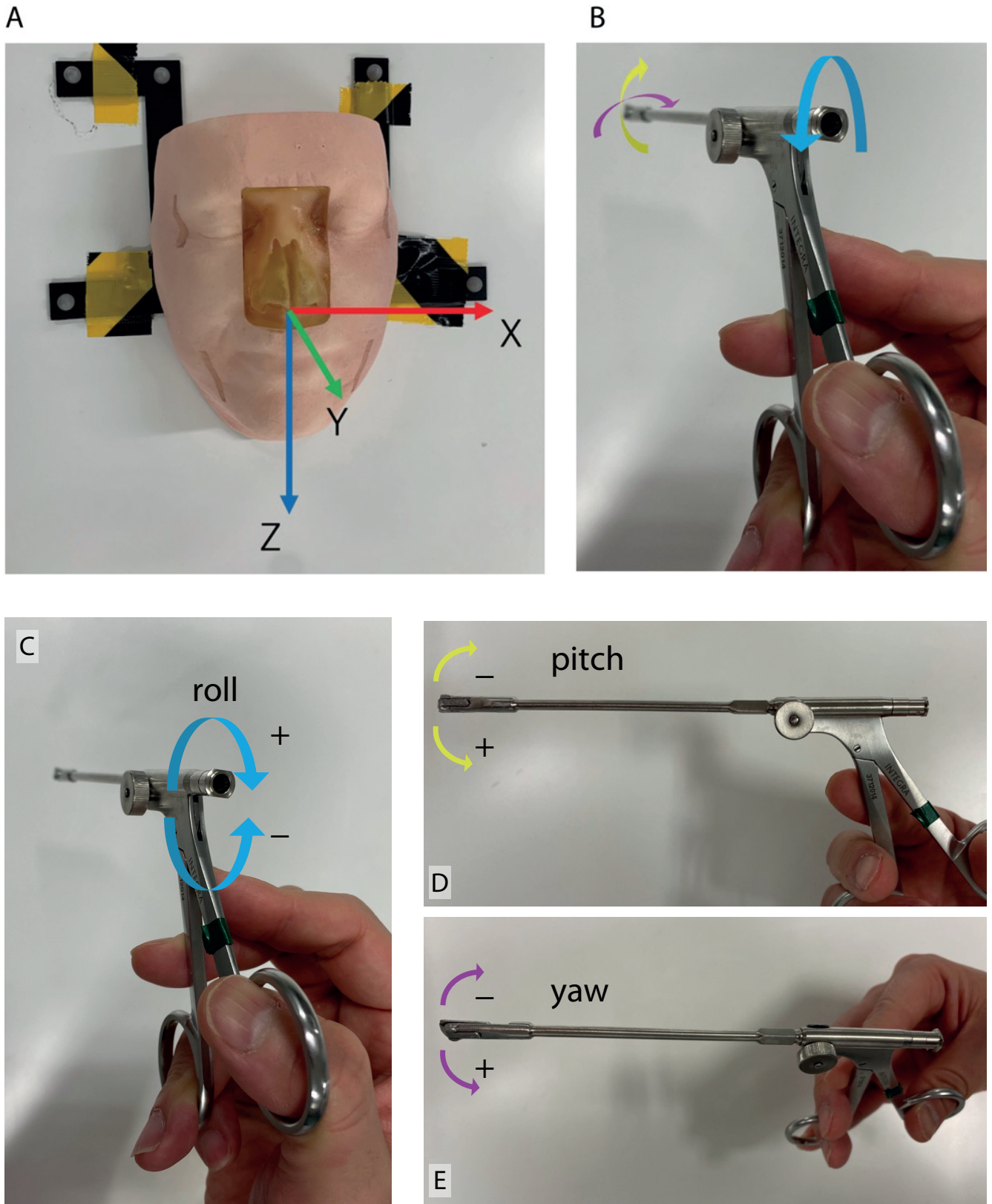


Figure 3. (A) The definition of the Cartesian coordinate system in the study. The x-, y- and z-axes were defined as right-to-left (the red arrow), ventral-dorsal (the green arrow) and cephalon-caudal directions (the blue arrow). (B) The definition of the motion in the angular coordinate system in the study. The sky-blue, yellow, and purple arrows stand for roll, pitch, and yaw, respectively. (C) The rotation in roll axis was defined as the rotation around the long axis of the forceps (a circular movement; the sky-blue arrow). (D) The rotation in the pitch axis was defined around the side-to-side axis of the forceps (tips' up and down movement; the yellow arrow). (E) The rotation in the yaw axis was defined as the rotation around the vertical axis of the forceps (tips' movement from side to side; the purple arrow).

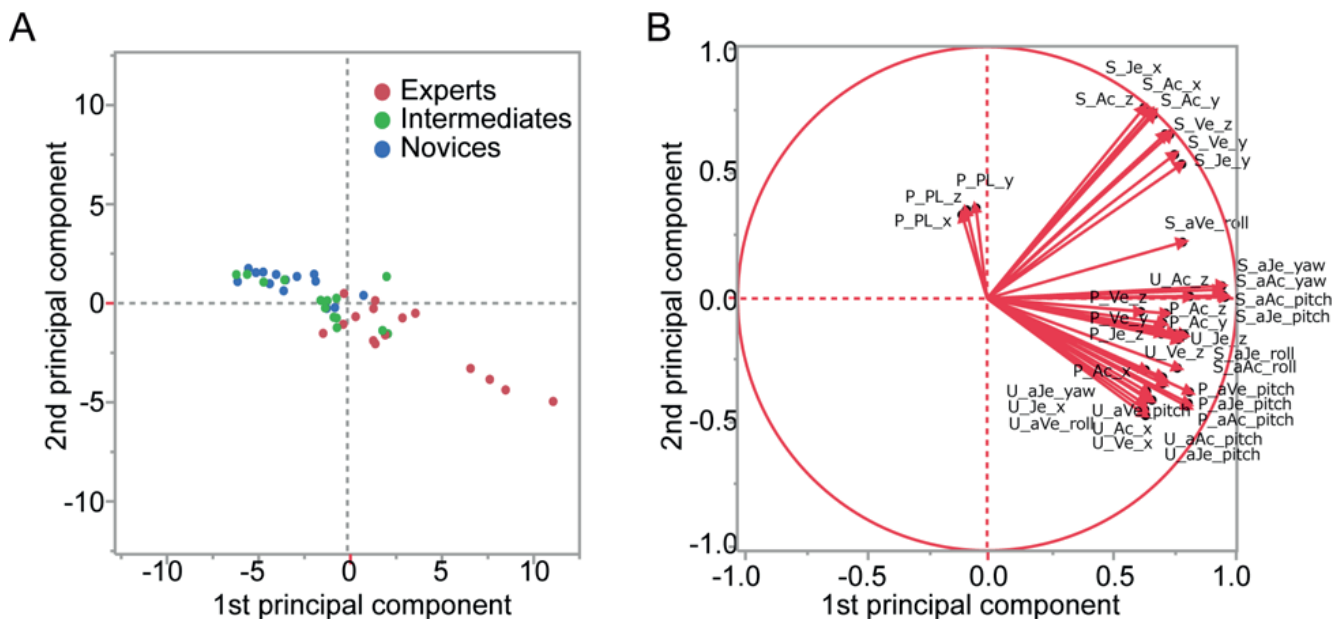


Figure 4. Principal component analysis regarding the groups with different levels of surgical skill. (A) The principal component score plots. (B) The Loading plots of 1st and 2nd principal components. P: Pediatric backbiter forceps, S: Straight-cutting forceps, U: Upturned-cutting forceps, PL: Path length, Ve: Velocity, Ac: Acceleration, Je: Jerk, aVe: angular velocity, aAc: angular acceleration, aJe: angular Jerk, x: x-axis, y: y-axis, z: z-axis, roll: roll-axis, pitch: pitch-axis, and yaw: yaw-axis.

angular coordinate system (Figure 3). The Cartesian coordinate system is the world coordinate system, independently of the posture of the instruments. The x-, y-, and z-axes in the Cartesian were defined as right-to-left, ventral-dorsal, and cephalon-caudal directions, respectively (Figure 3A). The angular coordinate system was the system defined by the posture of the instruments and consisted of the roll, pitch, and yaw axes (Figure 3B); The rotation in the roll axis was defined as the rotation around the long axis of the forceps (a circular movement). The rotation in the pitch axis was defined around the side-to-side axis of the forceps (tips up and down). The rotation in the yaw axis was defined as the rotation around the vertical axis of the forceps (tips move from side to side).

In this study, the following motion metrics in the Cartesian coordinate system were analyzed; total path length of the tip trajectory (m) of instruments, and average velocity (m/s), acceleration, acceleration (m/s²), and jerk (m/s³) of the tip of instruments. Jerks are a further derivative of acceleration and represent the smoothness of movement. In the angular coordinate system, average angular velocity vector (rad/s), angular acceleration vector (rad/s²), and angular jerk vector (rad/s³) were calculated. Greater detail is given in the supplementary materials and methods.

Analysis and statistics

Shapiro-Wilk tests were applied to evaluate whether the data fitted a normal distribution curve. The data that was normally distributed was expressed as mean (± SD), and the data not

normally distributed was expressed as median with the inter-quartile range. Parametric data were assessed with one-way ANOVA followed by Tukey’s test among three or more groups. Non-parametric data were assessed with the Kruskal-Wallis test followed by the Mann-Whitney U among the groups. The paired Wilcoxon test was utilized for comparison before and after the repetitive training. P values of less than 0.05 were considered statistically significant.

Principal component analysis (PCA) was performed using the metrics showing significant differences to examine which metrics contribute to the differentiation of the surgical skills. The analysis is a data reduction technique used to summarize an abundant number of variables to a small number of important and relevant features (principal components). The results were expressed in the score plot and the loading plot. The score plot was a data projection onto two-dimensional coordinates with the first principal component on the x-axis and the second principal component on the y-axis. The loadings plot demonstrated the relationship between the primary components and the original variables. More details on PCA are provided in supplementary materials and methods. All the analyses were performed using JMP 11 (SAS Institute Inc. Cary, NC, USA).

Results

Characteristics of participants and the deficient ratio of the data

Forty-seven otolaryngologists participated the present study. The characteristics of the participants are shown in Table S1.

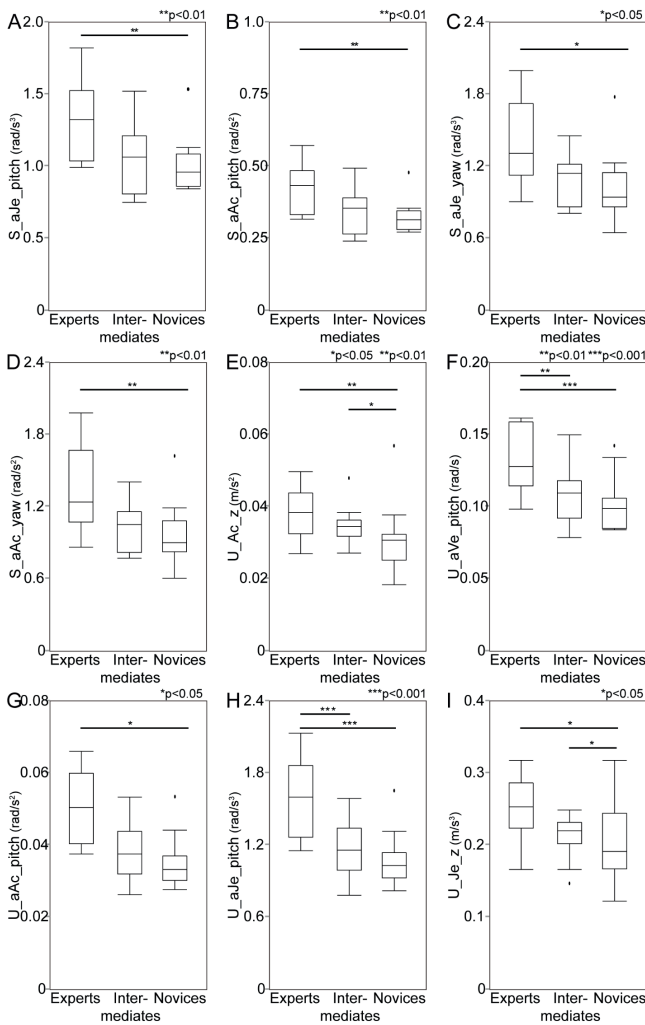


Figure 5. Motion metrics which significantly contributed to the first principal component in the principal component analysis regarding the groups with different levels of surgical skill. (A) Angular jerk of the straight forceps in the pitch axis, (B) Angular acceleration of the straight forceps in the pitch axis, (C) Angular jerk of the straight forceps in the yaw axis, (D) Angular acceleration of the straight forceps in the yaw axis, (E) Acceleration of the upturned-cutting forceps in the z-axis, (F) Angular velocity of the upturned-cutting forceps in the pitch axis, (G) Angular acceleration of the upturned-cutting forceps in the pitch axis, (H) Angular jerk of the upturned-cutting forceps in the pitch axis, (I) Jerk of the upturned-cutting forceps in the z-axis. S: Straight-cutting forceps, U: Upturned-cutting forceps, Je: Jerk, aVe: angular velocity, aAc: angular acceleration, aJe: angular Jerk, pitch: pitch-axis, and yaw: yaw-axis.

As the motion capture system froze during one mock surgery, only 46 surgeries (97.87%) could be analyzed in the present study. The motion metrics of the endoscope were missing $0.003 \pm 0.01\%$ of the time used. Similarly, the deficient ratio of the pediatric backbiter forceps, the straight-cutting forceps, and the upturned-cutting forceps were $0.69 \pm 2.4\%$, $4.54 \pm 14.0\%$, and $0.88 \pm 1.8\%$. The participants' perceived degree of interference

of the infrared markers to the surgeries (0: not at all to 100: completely interfered) was 18.45 ± 22.56 for the endoscope and 22.68 ± 24.73 for the forceps, respectively.

The motion metrics showing significant differences among the groups (Table S2, S3, S4, and S5, and Figure 4 and 5)

There were significant differences between the experts and the other groups in 24 out of 48 (50%) motion metrics analyzed in the present study. The motion metrics of the upturned-cutting forceps was faster in the expert group than the others in the x-axis (the velocity, the acceleration, and the jerk) and z-axis (the velocity, the acceleration, and the jerk) in the Cartesian coordinate system (Table S2). Superiority of the experts over the other groups was also found in the angular coordinate system, in the roll axis (the angular velocity, acceleration, and jerk), in the pitch axis (the angular velocity, acceleration, and jerk), and in the yaw axis (the angular jerk). There was no significant difference in the path length of the upturned-cutting forceps.

As for the straight-cutting forceps, all metrics (the velocity, acceleration, and jerk) in the x-, y-, and z-axes in the Cartesian coordinate system were significantly faster in the experts (Table S3). Most metrics in the angular coordinate system were also higher in the experts than the novices in the roll axis (the angular velocity, acceleration, and jerk), in the pitch axis (the angular acceleration and jerk), in the yaw axis (the angular acceleration and jerk). There was no significant difference in the path length of the straight-cutting forceps.

Also, experts showed superiority in handling the pediatric backbiter forceps over the other in the x-axis (the acceleration), the y-axis (the velocity and acceleration), the z-axis (the velocity, acceleration, and jerk), and in the pitch axis (the angular velocity, acceleration, and jerk, Table S4). The path length of the backbiter was significantly longer in the novices than in the other groups.

There were no significant differences among the groups in any metrics regarding the endoscope in the Cartesian and angular coordinate systems (Table S5).

Primary component analysis identified the motion metrics reflecting the different levels of surgical skill

Figure 4 shows the results of PCA regarding the group with different levels of surgical skill. The experts were mainly distributed from the right side to the middle, the intermediates in the middle, and the novices from the middle to the left. The 1st, 2nd, and 3rd principal components explained 51.9%, 16.9%, and 10.8% of the total variance, respectively. The 1st principal component was the most strongly affected by angular acceleration and jerk of the straight forceps in the pitch and yaw axis, followed by the acceleration of the upturned-cutting forceps in the z-axis, and the angular velocity, acceleration, and jerk of the upturned-cutting forceps in the pitch axis (Figure 5 and Table

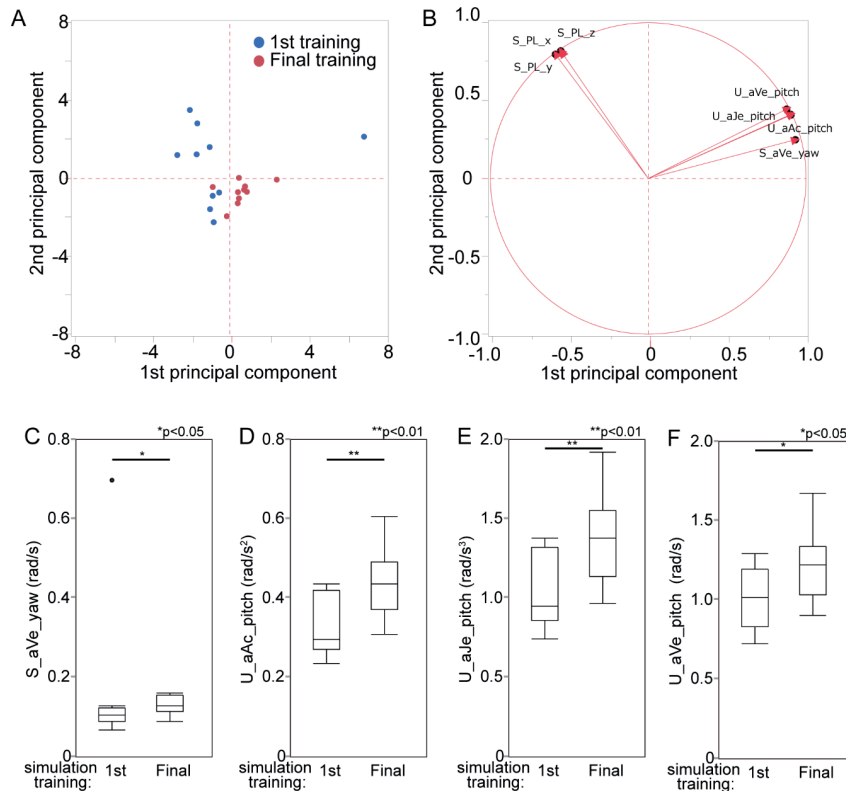


Figure 6. Motion analysis in the training study. (A) The principal component score plots. Blue dots: the 1st training, Red dots: the final training. (B) The Loading plots of 1st and 2nd principal components. (C-F) Motion metrics which significantly contributed to the first principal component in the principal component analysis in the training study. (C) Angular velocity of the straight forceps in the yaw axis, (D) Angular acceleration of the upturned-cutting forceps in the pitch axis, (E) Angular jerk of the upturned-cutting forceps in the pitch axis, (F) Angular velocity of the upturned-cutting forceps in the forceps-in the pitch axis. P: Pediatric backbiter forceps, S: Straight-cutting forceps, U: Upturned-cutting forceps, PL: Path length, aVe: angular velocity, aAc: angular acceleration, aJe: angular Jerk, x: x-axis, y: y-axis, z: z-axis, pitch: pitch-axis, and yaw: yaw-axis.

S6). The 2nd principal component mainly consists of the motion of the straight forceps in the Cartesian coordinate system, and the 3rd component did the path length of pediatric backbiters. These results suggested that these motion metrics, especially the angular movements of the forceps, reflects different surgical skill levels well.

Change of the motion metrics by registrars’ repetitive surgical training

Next, it was examined how motion metrics changed as registrars repeated surgical training: ten otolaryngology registrars repeated the surgeries six times on the models as part of their repetitive training. Their improvement in surgical skills has been validated previously (3). Significant changes after the trainings were found in 7 out of the 48 metrics: the path length of the pediatric backbiter forceps (x-, y-, and z-axis), the angular velocity of the straight forceps in the yaw axis, and the angular velocity, acceleration, and jerk of the upturned-cutting forceps in the pitch-axis (Table S7). Overall, the path lengths got significantly shorter and the angular motions faster, like the experts in the above investigation. However, no motion metrics of the forceps

changed when measured in the Cartesian coordinate system. There were no significant differences in the metrics related to the endoscope movement in the Cartesian or the angular coordinate system.

The metrics that showed significant differences were subjected to primary component analysis (Figure 6). The 60.3% and 36.4% of the total variances were explained with the first and second principal components, respectively. The first principal component was mostly affected by the angular velocity of the straight forceps in the yaw axis, followed by the angular motion of the upturned-cutting forceps (Figure 6 and Table S8). The second principal component consists of the path lengths of the pediatric backbiter forceps. These results support the improvement in surgical skill of the registrars through the repetitive training.

Discussion

The assessment of surgical skill has remained and enigma for accreditation by colleges around the world. To test surgical skill surgeons have used cadavers. One of the major confounding factors has been the variability in the anatomy of cadavers as

the surgical skill of the various surgeons been examined cannot be compared if the anatomy on which they are operating is different. In this study this was overcome by using validated high fidelity 3D printed models constructed from the actual anatomy of patients. This allowed the same anatomy to be given to all surgeons therefore allowing surgical skill levels to be compared. This is the first study we are aware of where simultaneous motion tracking of multiple surgical instruments during ESS has been recorded and analyzed. This study has shown that surgical skill levels differ depending upon the level of the surgeon and in the registrar group that skill levels can improve with repetitive training.

Previous research using motion tracking to evaluate surgical performances during ESS was done using a commercially available image guidance system⁽¹⁸⁾. In this study, six otolaryngology experts and nine registrars performed ethmoidectomies on actual patients and the motion of the endoscope and surgical instruments were analyzed based on the position data measured with the image guidance system. However, as the surgeries were performed in actual patients with different anatomies, the motions could not be measured under the same conditions. Further, the frame rate was limited (5 frames/sec) as the image guide system was not designed especially for motion tracking. The motion metrics were analyzed for the sum of motion of all the instruments, not for each instrument, individually. The analysis was not done separately for each axis (x-, y-, and z-axis in the Cartesian coordinate system and roll-, pitch-, and yaw-axis in the angular coordinate system), but for all axes together. Our study was performed under the standardized conditions provided by the 3D models. The high-speed motion capture system allowed for high quality and speed of motion tracking as high as 100 frames/sec. Further, by being attached to different patterns of infrared markers, different surgical instruments were measured and separately analyzed. The movement of instruments was also analyzed individually on each axis. This provided more detailed findings on surgeons' hand maneuvers during ESS. Overall, the experts demonstrated superiority in handling the forceps in speeds, accelerations, and jerks to novices, but not the endoscope. The principal component analysis in the different groups identified the following motion metrics as the main contributor to the first principal component; 1) angular motion of the straight forceps in the pitch and yaw axis, 2) the linear acceleration of the upturned-cutting forceps in the z-axis, and 3) the angular motion of the upturned-cutting forceps in the pitch axis. This means that these metrics varied most largely among the surgeons with different surgical skills, suggesting being possible indicators of surgical skills. All these motions corresponded to the movement needed to adjust the tip of forceps to the structure to be resected and are frequently repeated during ESS procedures. Such fine manipulation within the limited space of

the nasal cavity under the planar view of 2D monitors required highly trained visual-spatial and motor skills. As these metrics were different for the different skill groups they indicated the various surgical skill levels. This finding was also supported by the results from the training cohort showing that some of these metrics improved as the registrars trained.

In this study, the hand maneuver was analyzed not only in the Cartesian coordinate system but also in the angular coordinate system. Therefore, the same motion could be differently analyzed in the two coordinates, depending on the posture of forceps. For example, when the forceps are pointed in a cephalic direction, the pitch axis corresponds to the z-axis of the Cartesian coordinates, whereas when the forceps are pointed sideways, the pitch axis corresponds to the y-axis of the Cartesian coordinates.

The principal component analysis revealed that the metrics in the angular coordinate system largely contributed to the first principal components rather than those in the Cartesian coordinate system. In addition, the skill improvement in the training study was not detected in the metrics in the Cartesian coordinate system but in the angular coordinate system. Therefore, the angular coordinate system could be more suitable for analyzing hand maneuvers for ESS than the Cartesian coordinate system. As the forceps for ESS are designed to be held in a pistol-like fashion, the radial and ulnar flexion of the hand corresponds to the movement of the pitch axis of the forceps. Similarly, the palmar dorsiflexion corresponds to the yaw axis, and the radial and palmar abduction to the roll axis. We speculated that the hand movement, an angular movement with the wrist as the axis, is reflected in an angular movement of the forceps more directly than as linear movement in the Cartesian coordinates.

It should be noted that the insertion and desertion of surgical instruments (the motion relative to the world coordinate system) cannot be evaluated in the angular coordinate system. This was why the Cartesian coordinate system analysis was also necessary, although neither differences among the different groups nor improvements through the training were found in metrics in the Cartesian coordinate system.

As well as acceleration, jerk also markedly contributed to the first principal component on the PCA analysis. Jerks are a further derivative of acceleration and represent the smoothness of movement. There are many reports identifying the jerk as the indicator of surgical skill. Faster jerks are related to dexterous skill in laparoscopy⁽⁴⁾ and central venous access procedures⁽¹³⁾, while slower jerks indicated matured skills in arthroscopy⁽¹⁰⁾, bipolar hemostasis⁽¹¹⁾, transcatheter aortic valve implantation⁽¹²⁾, obstetric ultrasound echoes⁽¹⁴⁾ and bipolar ablation⁽¹⁵⁾. In cases of ESS, the movement of cutting forceps is not a big motion with a long stroke but a collective of repetitive small motions with a shorter

pathway. Experts would repeat this fine manipulation of forceps more efficiently, and this may have resulted in the experts' 'less smoothness' with a higher jerk than the others.

The path length of the instruments did not significantly distinguish between different skill levels other than with the pediatric back biters where the path length was significantly longer in the novices and shortened after the training. The pediatric backbiter forceps were utilized only once for a specific task, the uncinectomy. The shortened path length in the experts and in the registrars after training would reflect the higher efficiency in the uncinectomy.

Endoscopy was not a differentiating factor between the groups or change in the training study. Different skill levels might be reflected in the location of an endoscope, not in its movement. It is possible that our methods were not sensitive enough to detect the differences. Further studies are necessary to optimize the analysis of the endoscope's movement.

This study has several limitations. Firstly, the number of surgical instruments analyzed in this study was limited. Secondly, the infrared markers attached to the instruments could have affected the ability of the surgeon to perform certain tasks. Thirdly, the system measures only performance based on time-dependent manner and smoothness of movement, which is just one factor of skill acquisition in ESS. For example, complications could not be evaluated with the system. However, this study is a useful start to the objective evaluation of surgical education in ESS.

Conclusion

Combined with the validated 3D-printed sinus models, the motion capture system provided the objective evaluation of the surgical performances of ESS.

Acknowledgement

We thank Dr. Aya Honma, Dr. Shogo Kimura, Ms. Shizuka Sugawara, Ms. Yuka Masuta, Ms. Yumiko Kimura, Mr. Kaito Yamada, and Mr. Minoru Ishida for their support in the surgical training course and in the writing of the manuscript. We are grateful to the members of the CAST committee at the Hokkaido University Hospital for their support. We would also like to thank KARL STORZ, Medtronic, and Stryker for providing the endoscopes, surgical equipment, instruments and the Building Block software.

Authors' contributions

KMi, MS, TA, AJP, PJW, and AK designed the project. MS, KMi, RW, TS, AN and AH organized the simulation training and collected data. MS and YN analyzed OSATS score. KMi, TS, KE, KMa, and AK analyzed motion metrics. KMi, MS, DH, AJP, and PJW wrote the draft. All authors provided feedback on the manuscript and gave final approval to the submitted paper.

Funding

This work was partially supported by JSPS Grant-in-Aid for Scientific Research JP18H04102 and 22K16923.

Conflicts of interest

PJW: consultant for Fusetec and receiving royalties from Fusetec. AJP: consultant for Fusetec, Medtronic, ENT technologies, Tissium, and Aerin Medical, shareholder of Chitogel, and speakers bureau for Sequiris. The remaining authors declare that the research was conducted in the absence of any commercial or financial relationships that could be construed as a potential conflict of interest.

References

- Fokkens WJ, Lund VJ, Hopkins C, et al. European Position Paper on Rhinosinusitis and Nasal Polyps 2020. *Rhinology*. 2020; 58(Suppl S29): 1-464.
- Wormald P-J. *Endoscopic sinus surgery*. Stuttgart, New York: Thieme. 2018.
- Suzuki M, Miyaji K, Watanabe R, et al. Repetitive simulation training with novel 3D-printed sinus models for functional endoscopic sinus surgeries. *Laryngoscope Investig Otolaryngol*. 2022; 7(4): 943-954.
- Ebina K, Abe T, Higuchi M, et al. Motion analysis for better understanding of psychomotor skills in laparoscopy: objective assessment-based simulation training using animal organs. *Surg Endosc*. 2021; 35(8): 4399-4416.
- Hwang H, Lim J, Kinnaird C, et al. Correlating motor performance with surgical error in laparoscopic cholecystectomy. *Surg Endosc*. 2006; 20(4): 651-655.
- Farcas MA, Trudeau MO, Nasr A, Gerstle JT, Carrillo B, Azzie G. Analysis of motion in laparoscopy: the deconstruction of an intracorporeal suturing task. *Surg Endosc*. 2017; 31(8): 3130-3139.
- Sánchez-Margallo JA, Sánchez-Margallo FM, Oropesa I, Enciso S, Gómez EJ. Objective assessment based on motion-related metrics and technical performance in laparoscopic suturing. *Int J Comput Assist Radiol Surg*. 2017; 12(2): 307-314.
- Shaharan S, Nugent E, Ryan DM, Traynor O, Neary P, Buckley D. Basic surgical skill retention: can patriot motion tracking system provide an objective measurement for it? *J Surg Educ*. 2016; 73(2): 245-249.
- Yamaguchi S, Yoshida D, Kenmotsu H, et al. Objective assessment of laparoscopic suturing skills using a motion-tracking system. *Surg Endosc*. 2011; 25(3): 771-775.
- Kholinne E, Gandhi MJ, Adikrishna A, et al. The dimensionless squared jerk: an objective parameter that improves assessment of hand motion analysis during simulated shoulder arthroscopy. *Biomed Res Int*. 2018; 2018: 7816160.
- Ghasemloonia A, Maddahi Y, Zareinia K, Lama S, Dort JC, Sutherland GR. Surgical skill assessment using motion quality and smoothness. *J Surg Educ*. 2017; 74(2): 295-305.
- Mazomenos EB, Chang PL, Rippel RA, et al. Catheter manipulation analysis for objective performance and technical skills assessment in transcatheter aortic valve implantation. *Int J Comput Assist Radiol Surg*. 2016; 11(6): 1121-1131.
- Villagrán I, Moëgne-Loccoz C, Aguilera V, et al. Biomechanical analysis of expert anesthesiologists and novice residents performing a simulated central venous access procedure. *PLoS One*. 2021; 16(4): e0250941.
- Dromey BP, Ahmed S, Vasconcelos F, et al. Dimensionless squared jerk: An objective differential to assess experienced and novice probe movement in obstetric ultrasound. *Prenat Diagn*. 2021; 41(2): 271-277.

15. Sakakura Y, Kamei M, Sakamoto R, et al. Biomechanical profiles of tracheal intubation: a mannequin-based study to make an objective assessment of clinical skills by expert anesthesiologists and novice residents. *BMC Med Educ.* 2018; 18(1): 293.
16. Lin SY, Laeeq K, Ishii M, et al. Development and pilot-testing of a feasible, reliable, and valid operative competency assessment tool for endoscopic sinus surgery. *Am J Rhinol Allergy.* 2009; 23(3): 354-359.
17. Ebina K, Abe T, Hotta K, et al. Objective evaluation of laparoscopic surgical skills in wet lab training based on motion analysis and machine learning. *Langenbecks Arch Surg.* 2022.
18. Sugino T, Nakamura R, Kuboki A, Honda O, Yamamoto M, Ohtori N. Comparative analysis of surgical processes for image-guided endoscopic sinus surgery. *Int J Comput Assist Radiol Surg.* 2019; 14(1): 93-104.

Masanobu Suzuki, M.D., Ph.D.
Department of Otolaryngology
Head and Neck Surgery
Faculty of Medicine and Graduate
School of Medicine
Hokkaido University
Kita 15, Nishi 7
Kita-ku
Sapporo
Hokkaido 060-8638
Japan

E-mail:
masanobuwork@med.hokudai.ac.jp

Kou Miyaji^{1,#}, Masanobu Suzuki^{2,#}, Ryosuke Watanabe², Takayoshi Suzuki²,
Kotaro Matoba³, Akira Nakazono², Yuji Nakamaru², Koki Ebina¹, Takashige Abe⁴,
Dominik Hinder⁵, A.J. Psaltis⁵, P.J. Wormald¹, Akihiro Homma², Atsushi Konno¹

Rhinology 63: 2, 190 - 199, 2025
<https://doi.org/10.4193/Rhin22.320>

Received for publication:

August 15, 2022

Accepted: December 10, 2024

Associate Editor:

Wytske Zwetsloot-Fokkens

[#] equally contributed to this work

¹ Graduate School of Information Science and Technology, Hokkaido University, Sapporo, Japan

² Department of Otolaryngology - Head and Neck Surgery, Faculty of Medicine and Graduate School of Medicine, Hokkaido University, Sapporo, Hokkaido, Japan

³ Department of Forensic Medicine, Faculty of Medicine and Graduate School of Medicine, Hokkaido University, Sapporo, Japan

⁴ Department of Urology, Hokkaido University Graduate School of Medicine, Hokkaido University, Sapporo, Hokkaido, Japan

⁵ Department of Surgery - Otorhinolaryngology Head and Neck Surgery, Central Adelaide Local Health Network and the University of Adelaide, Adelaide, SA, Australia

SUPPLEMENTARY MATERIAL

Supplementary materials and methods

Motion analysis

In this study, the following motion metrics were analyzed.

i) Path length (PL) (m): total length of the tip trajectory of an instrument.

$$\sum_{i=1}^{n-1} \sqrt{(x_{i+1} - x_i)^2 + (y_{i+1} - y_i)^2 + (z_{i+1} - z_i)^2}$$

Where n is the total number of frames, and x_i , y_i , and z_i are tip positions of an instrument in frame i . In this study, the trajectory that lies inside the 3D models is the measurement target, excluding that outside of them.

ii) velocity (m/s): average velocity of the tip of an instrument.

$$[v_x \ v_y \ v_z] = \frac{1}{n} \sum_{i=1}^n \left[\frac{dx_i}{dt} \ \frac{dy_i}{dt} \ \frac{dz_i}{dt} \right]$$

iii) acceleration (m/s²): average acceleration of the tip of an instrument.

$$[a_x \ a_y \ a_z] = \frac{1}{n} \sum_{i=1}^n \left[\frac{d^2x_i}{dt^2} \ \frac{d^2y_i}{dt^2} \ \frac{d^2z_i}{dt^2} \right]$$

iv) jerk (m/s³): average jerk of the tip of an instrument.

$$[j_x \ j_y \ j_z] = \frac{1}{n} \sum_{i=1}^n \left[\frac{d^3x_i}{dt^3} \ \frac{d^3y_i}{dt^3} \ \frac{d^3z_i}{dt^3} \right]$$

v) angular velocity vector (rad/s): average velocity vector of an instrument.

Motion capture data also measures the posture information of each instrument in world coordinates. The attitude information measured in this study is obtained at ZYX Euler angles $\theta = (\theta_z, \theta_y, \theta_x)$, and the rotation matrix R is calculated from the ZYX Euler angles. The angular velocity vector was calculated from the difference of the rotation matrices. The difference of the rotation matrix between the frame i and frame $i + k$ ($i = 1, \dots, n$) is calculated as follows.

$${}^iR_e[i] = R[i]^T R[i + k], \quad R[i + k] = R[n] \text{ for } i + k > n$$

Note that the difference of the rotation matrices ${}^iR_e[i]$ is defined with respect to the local (instrument's) coordinate frame.

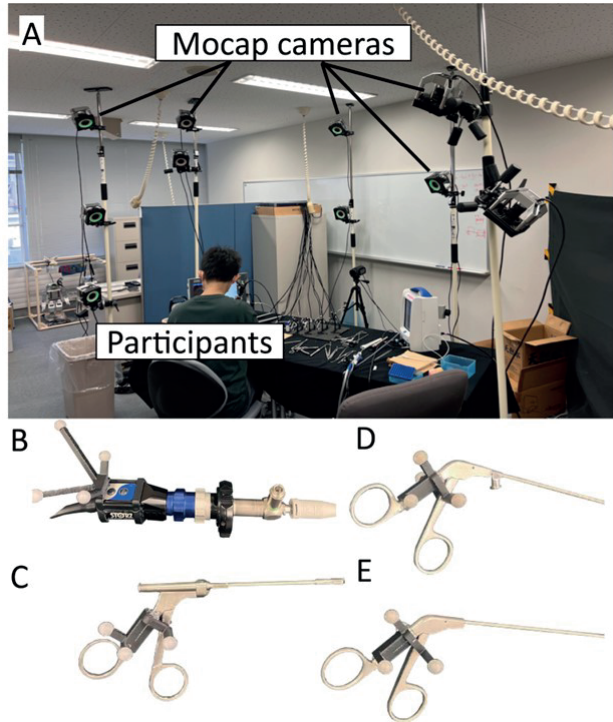


Figure S1. Photographs of the simulation training and the surgical instruments attached the infrared reflective markers. The motion capture system, which consisted of 11 infrared cameras, simultaneously tracked the movement of the endoscope and the forceps during the mock surgery (A). The infrared reflective markers were attached to the endoscope (B), the pediatric backbiter forceps (C), the straight-cutting forceps (D), and the upturned-cutting forceps (E).

The angular velocity vector ${}^i\omega[i]$ is expressed by the following equation.

$${}^i\omega[i] = \frac{1}{k\Delta t} (\log {}^iR_e[i])^V$$

where Δt is the sampling time, $(\log {}^iR_e[i])$ is the matrix logarithm⁽¹⁸⁾, and O^V is the operator defined by

$$\begin{bmatrix} 0 & -\omega_z & \omega_y \\ \omega_z & 0 & -\omega_x \\ -\omega_y & \omega_x & 0 \end{bmatrix}^V = \begin{bmatrix} \omega_x \\ \omega_y \\ \omega_z \end{bmatrix}$$

Since ${}^i\omega[i]$ is calculated from the difference of the rotation matrix between the frame i and frame $i + k$, ${}^i\omega[i]$ is the moving average of angular velocities of k frames. k was set to 20, and the sampling time Δt was 0.01s. ${}^i\omega[i]$ is defined with respect to the local (instrument's) coordinate frame.

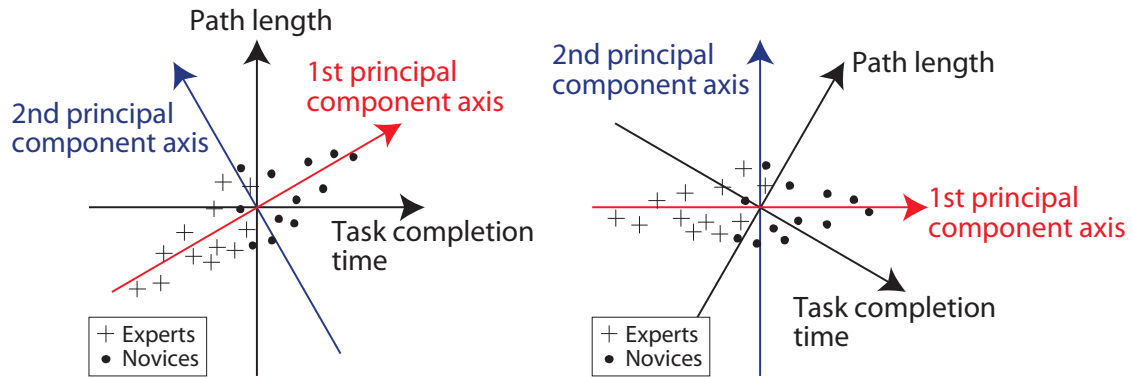


Figure S2. An example for explanation of principle component analysis.

vi) angular acceleration vector (rad/s²): average acceleration vector of an instrument.

$$\frac{d\omega}{dt}$$

vii) angular jerk vector (rad/s³): average jerk vector of an instrument.

$$\frac{d\omega^2}{d^2t}$$

In this study, the trajectory of the tip of an instrument (x^i, y^i , and z^i) was smoothed by the Savitzky-Golay filter, and its derivatives

$$\left(\frac{d^j x_i}{dt^j}, \frac{d^j y_i}{dt^j}, \text{ and } \frac{d^j z_i}{dt^j} (j = 1 \text{ to } 3)\right)$$

were also obtained by the filter. The polynomial order of the filter was set to 3, and the number of sampling frames of the filter was set to 101.

Principle component analysis

Principal component analysis is a data reduction technique used to summarize an abundant number of variables to a small number of important and relevant features (principal components). Suppose, hypothetically for example, experts tended to have shorter path lengths of surgical instruments and shorter task completion times (Figure S1). A normalized and dimensionless plot of the subject's surgical instrument path length and task completion time would be shown in the following Figure S1a. In principle component analysis, the first principal component axis is taken in the direction with the largest data variance. The second principal component axis is taken in the direction

with the second largest data variance and orthogonal to the first principal component axis. The value of the first principal component axis for each data best represents the characteristics of each data as illustrated in Figure S1b. Hence the two-dimensional data can be approximated by the one-dimensional data. In the first versus second principal components plot, original axes correspond to the loading plot. As described in the above example, the characteristics of many-dimensional data can be explained by several principal components.

In the example in Figure S2, it is supposed that experts (+) tend to have shorter path lengths of surgical instruments and shorter task completion times than novices (dot).

a) The data of experts and novices are plotted in the rectilinear coordinates, where the x-axis and y-axis represent task completion time and path length, respectively. The first principal component axis (red) is taken in the direction with the largest data variance. The second principal (blue) component axis is taken in the direction with the second largest data variance and orthogonal to the first principal component axis.

b) The data are re-plotted in the new coordinates where the first principal component axis (red) and the second principal component (blue) are taken as the x-axis and y-axis, respectively. Here, the two sorts of variables (task completion time and path length) are approximated by one data (the value of the first principal component axis). By repeating this process, many variables can be summarized into a small number of important and relevant features. The symbol of + and dot represents experts and novices, respectively.

Table S1. Characteristics of participants in the present study.

	Experts (n=15)	Intermediates (n=15)	Novices (n=16)	ANOVA/ Kruskal-Wallis	P value		
					Experts vs. Intermediates	Intermediates vs. Novices	Experts vs. Novices
OSATS score	72.93 ± 4.35	55.20 ± 3.67	38.38 ± 7.27	<0.001	<0.001	<0.001	<0.001
Experienced years (ave.)	17.87 ± 8.69	10.13 ± 5.91	4.50 ± 5.35	<0.001	0.009	0.065	<0.001
Gender (F/M)	1/14	1/14	4/12				
Dominant hand (Right/Left)	15/0	15/0	15/1				
Experienced ESS cases (ave.)	598.67 ± 764.96	56.27 ± 39.93	8.25 ± 13.89	<0.001	0.001	0.942	<0.001

Table S2. The measurement metrics of the upper-cutting forceps.

	Experts (n=15)	Intermediates (n=15)	Novices (n=16)	ANOVA/ Kruskal- Wallis	P value		
					Experts vs. Intermedi- ates	Intermedi- ates vs. Novices	Experts vs. Novices
Path length (m)							
X-axis	2.014 (1.487-3.111)	2.076 (1.585-2.567)	1.192 (0.5601-2.368)	0.074	0.455	0.144	0.028
Y-axis	3.337 (2.228-4.501)	3.115 (2.784-3.922)	1.771 (1.126-3.392)	0.143	1	0.133	0.066
Z-axis	3.683 (2.741-4.469)	3.5733 (2.929-4.083)	1.786 (1.1743-3.910)	0.130	0.868	0.155	0.050
Velocity (m/s)							
X-axis	0.007 (0.006-0.009)	0.006 (0.006-0.007)	0.005(0.005-0.007)	0.026	0.047	0.527	0.014
Y-axis	0.010 (0.009-0.013)	0.010 (0.009-0.011)	0.010 (0.008-0.011)	0.382	0.499	0.678	0.147
Z-axis	0.012 (0.011-0.013)	0.010 (0.010-0.011)	0.010 (0.008-0.011)	0.011	0.047	0.058	0.013
Acceleration (m/s²)							
X-axis	0.023 (0.022-0.031)	0.021 (0.019-0.023)	0.019 (0.016-0.021)	0.002	0.011	0.371	0.001
Y-axis	0.028 (0.023-0.036)	0.027 (0.024-0.030)	0.026 (0.020-0.029)	0.201	0.395	0.371	0.082
Z-axis	0.039 (0.033-0.044)	0.035 (0.032-0.036)	0.031 (0.025-0.033)	0.003	0.058	0.034	0.002
Jerk (m/s³)							
X-axis	0.171 (0.159-0.220)	0.150 (0.144-0.169)	0.132 (0.117-0.180)	0.007	0.011	0.326	0.008
Y-axis	0.209 (0.173-0.260)	0.200 (0.162-0.221)	0.195 (0.153-0.223)	0.335	0.266	0.948	0.171
Z-axis	0.254 (0.225-0.287)	0.221 (0.203-0.233)	0.192 (0.168-0.245)	0.016	0.020	0.499	0.013
Angle velocity (rad/s)							
Roll-axis	0.241 (0.203-0.259)	0.215 (0.144-0.222)	0.178 (0.157-0.203)	0.006	0.031	0.752	0.001
Pitch-axis	0.128 (0.116-0.146)	0.108 (0.093-0.118)	0.099 (0.085-0.103)	<0.001	0.003	0.304	<0.001
Yaw-axis	0.089 (0.082-0.105)	0.085 (0.072-0.095)	0.080 (0.073-0.092)	0.244	0.213	0.782	0.118
Angle acceleration (rad/s²)							
Roll-axis	0.786 (0.666-0.861)	0.618 (0.459-0.726)	0.501 (0.484-0.560)	<0.001	0.010	0.429	<0.001
Pitch-axis	0.503 (0.429-0.571)	0.372 (0.320-0.431)	0.333 (0.301-0.356)	<0.001	<0.001	0.304	<0.001
Yaw-axis	0.342 (0.291-0.382)	0.287 (0.241-0.341)	0.297 (0.254-0.314)	0.072	0.097	1.0000	0.026
Angle Jerk (rad/s³)							
Roll-axis	2.430 (2.056-2.683)	1.851 (1.407-2.263)	1.510 (1.500-1.716)	<.001	0.011	0.343	<0.001
Pitch-axis	1.596 (1.340-1.803)	1.138 (0.995-1.313)	1.032 (0.925-1.099)	<0.001	<0.001	0.286	<0.001
Yaw-axis	1.085 (0.906-1.239)	0.888 (0.742-1.063)	0.901 (0.798-0.977)	0.049	0.075	1.000	0.017

Table S3. The measurement metrics of the straight-cutting forceps.

	Experts (n=15)	Intermediates (n=15)	Novices (n=16)	ANOVA/ Kruskal- Wallis	P value		
					Experts vs. Intermedi- ates	Intermedi- ates vs. Novices	Experts. vs. Novices
Path length (m)							
X-axis	0.674 (0.411-1.082)	0.900 (0.522-1.415)	0.313 (0.004-1.226)	0.201	0.407	0.072	0.416
Y-axis	1.122 (0.594-1.925)	1.524 (0.776-2.318)	0.527 (0.012-1.765)	0.182	0.281	0.092	0.331
Z-axis	1.140 (0.628-1.795)	1.510 (0.743-2.102)	0.518 (0.011-1.782)	0.174	0.245	0.078	0.439
Velocity (m/s)							
X-axis	0.009 (0.008-0.012)	0.007 (0.006-0.009)	0.007 (0.005-0.008)	0.014	0.008	0.738	0.021
Y-axis	0.013 (0.013-0.019)	0.011 (0.011-0.013)	0.011 (0.010-0.013)	0.013	0.004	0.700	0.036
Z-axis	0.015 (0.013-0.017)	0.011 (0.010-0.014)	0.010 (0.0100-0.012)	0.006	0.002	0.625	0.021
Acceleration (m/s²)							
X-axis	0.035 (0.029-0.049)	0.023 (0.021-0.027)	0.024 (0.017-0.029)	0.005	0.002	0.939	0.011
Y-axis	0.041 (0.034-0.054)	0.031 (0.029-0.035)	0.028 (0.026-0.037)	0.007	0.003	0.625	0.021
Z-axis	0.055 (0.039-0.065)	0.035 (0.031-0.042)	0.035 (0.030-0.038)	0.007	0.002	0.939	0.024
Jerk (m/s³)							
X-axis	0.236 (0.213-0.336)	0.171 (0.149-0.220)	0.179 (0.135-0.232)	0.020	0.011	1	0.028
Y-axis	0.295 (0.230-0.383)	0.225 (0.175-0.260)	0.206 (0.188-0.259)	0.025	0.011	0.857	0.041
Z-axis	0.339 (0.280-0.383)	0.233 (0.185-0.267)	0.209 (0.196-0.251)	0.007	0.002	0.898	0.028
Angle velocity (rad/s)							
Roll-axis	0.224 (0.205-0.257)	0.169 (0.149-0.196)	0.170 (0.152-0.193)	0.015	0.014	0.464	0.015
Pitch-axis	0.1110 (0.094-0.135)	0.101 (0.079-0.105)	0.089 (0.086-0.100)	0.080	0.245	0.227	0.034
Yaw-axis	0.103 (0.100-0.127)	0.091 (0.080-0.098)	0.086 (0.079-0.098)	0.055	0.062	0.313	0.041
Angle acceleration (rad/s²)							
Roll-axis	0.700 (0.608-0.759)	0.508 (0.414-0.582)	0.490 (0.413-0.536)	0.004	0.020	0.153	0.002
Pitch-axis	0.389 (0.331-0.475)	0.342 (0.276-0.376)	0.313 (0.282-0.343)	0.018	0.213	0.088	0.007
Yaw-axis	0.384 (0.364-0.455)	0.330 (0.272-0.371)	0.299 (0.269-0.334)	0.013	0.062	0.096	0.009
Angle Jerk (rad/s³)							
Roll-axis	2.243 (1.761-2.375)	1.534 (1.178-1.781)	1.5337 (1.2328-1.630)	0.005	0.025	0.234	0.003
Pitch-axis	1.237 (1.037-1.500)	1.037 (0.849-1.174)	0.960 (0.881-1.067)	0.016	0.135	0.113	0.007
Yaw-axis	1.246 (1.136-1.473)	1.026 (0.845-1.148)	0.927 (0.836-1.053)	0.014	0.056	0.113	0.010

Table S4. The measurement metrics of the pediatric back-biter forceps.

	Experts (n=15)	Intermediates (n=15)	Novices (n=16)	ANOVA/ Kruskal- Wallis	P value		
					Experts vs. Intermedi- ates	Intermedi- ates vs. Novices	Experts. vs. Novices
Path length (m)							
X-axis	0.389 (0.209-0.609)	0.279 (0.176-0.712)	0.887 (0.635-1.089)	< 0.001	0.590	0.001	0.002
Y-axis	0.598 (0.301-0.830)	0.350 (0.190-0.951)	1.306 (0.834-1.581)	0.001	0.481	0.001	0.002
Z-axis	0.436 (0.250-0.676)	0.344 (0.213-0.770)	1.138 (0.727-1.434)	< 0.001	0.431	< 0.001	0.001
Velocity (m/s)							
X-axis	0.006 (0.006-0.007)	0.006 (0.004-0.007)	0.005 (0.005-0.006)	0.278	0.362	0.890	0.086
Y-axis	0.009 (0.007-0.011)	0.007 (0.006-0.009)	0.008 (0.007-0.009)	0.028	0.016	0.374	0.046
Z-axis	0.008 (0.007-0.010)	0.007 (0.005-0.008)	0.007 (0.006-0.008)	0.045	0.020	0.213	0.138
Acceleration (m/s²)							
X-axis	0.022 (0.017-0.029)	0.018 (0.014-0.021)	0.016 (0.014-0.021)	0.048	0.056	0.828	0.023
Y-axis	0.028 (0.020-0.033)	0.0190 (0.016-0.022)	0.020 (0.018-0.023)	0.010	0.004	0.374	0.038
Z-axis	0.0315 (0.026-0.041)	0.023 (0.019-0.027)	0.022 (0.020-0.028)	0.003	0.002	0.767	0.007
Jerk (m/s³)							
X-axis	0.160 (0.138-0.199)	0.143 (0.101-0.193)	0.131 (0.109-0.165)	0.097	0.171	0.621	0.031
Y-axis	0.713 (0.148-0.223)	0.148 (0.122-0.157)	0.147 (0.129-0.172)	0.135	0.056	0.418	0.213
Z-axis	0.183 (0.150-0.239)	0.152 (0.123-0.178)	0.146 (0.130-0.178)	0.021	0.020	0.984	0.015
Angle velocity (rad/s)							
Roll-axis	0.235 (0.208-0.276)	0.211 (0.168-0.251)	0.225 (0.180-0.246)	0.111	0.089	0.984	0.060
Pitch-axis	0.112 (0.099-0.121)	0.093 (0.073-0.103)	0.083 (0.079-0.088)	0.003	0.005	0.767	0.002
Yaw-axis	0.125 (0.114-0.134)	0.107 (0.086-0.131)	0.105 (0.096-0.127)	0.154	0.135	0.890	0.072
Angle acceleration (rad/s²)							
Roll-axis	0.692 (0.633-0.883)	0.649 (0.469-0.714)	0.649 (0.581-0.667)	0.100	0.074	0.953	0.060
Pitch-axis	0.354 (0.293-0.412)	0.319 (0.237-0.347)	0.277 (0.254-0.328)	0.020	0.031	0.984	0.009
Yaw-axis	0.421 (0.362-0.495)	0.339 (0.244-0.464)	0.348 (0.324-0.442)	0.130	0.115	0.514	0.072
Angle Jerk (rad/s³)							
Roll-axis	2.093 (2.007-2.683)	1.872 (1.439-2.179)	1.991 (1.757-2.052)	0.060	0.046	0.540	0.046
Pitch-axis	1.137 (0.935-1.277)	1.020 (0.721-1.067)	0.853 (0.783-1.030)	0.024	0.051	0.828	0.008
Yaw-axis	1.302 (1.103-1.568)	1.041 (0.741-1.425)	1.072 (0.997-1.360)	0.104	0.089	0.465	0.066

Table S5. The measurement metrics of the endoscope.

	Experts (n=15)	Intermediates (n=15)	Novices (n=16)	ANOVA/ Kruskal- Wallis	P value		
					Experts vs. Intermedi- ates	Intermedi- ates vs. Novices	Experts. vs. Novices
Path length (m)							
X-axis	3.64 (3.14-4.21)	3.88 (3.11-4.99)	4.10 (3.39-4.47)	0.844	0.836	0.828	0.540
Y-axis	9.67 (8.61-11.53)	9.01 (7.94-11.16)	8.57 (7.22-10.68)	0.520	0.362	0.621	0.353
Z-axis	9.37 (7.44-9.80)	8.94 (6.45-10.07)	8.18 (7.01-9.54)	0.446	0.481	0.621	0.213
Velocity (m/s)							
X-axis	0.002 (0.002-0.002)	0.002 (0.001-0.002)	0.002 (0.001-0.002)	0.926	0.648	0.859	0.828
Y-axis	0.005 (0.004-0.006)	0.004 (0.003-0.005)	0.004 (0.003-0.005)	0.351	0.199	0.797	0.244
Z-axis	0.004 (0.004-0.005)	0.004 (0.003-0.005)	0.004 (0.003-0.004)	0.398	0.340	0.953	0.185
Acceleration (m/s²)							
X-axis	0.006 (0.005-0.006)	0.005 (0.004-0.007)	0.007 (0.004-0.007)	0.955	0.934	0.890	0.767
Y-axis	0.013 (0.010-0.017)	0.010 (0.009-0.014)	0.011 (0.008-0.014)	0.244	0.263	0.540	0.118
Z-axis	0.013 (0.010-0.017)	0.011 (0.008-0.015)	0.011 (0.009-0.014)	0.382	0.320	0.890	0.185
Jerk (m/s³)							
X-axis	0.042 (0.038-0.046)	0.040 (0.030-0.050)	0.42 (0.031-0.047)	0.968	0.772	1	0.921
Y-axis	0.087 (0.067-0.099)	0.069 (0.055-0.091)	0.076 (0.056-0.091)	0.342	0.199	0.984	0.228
Z-axis	0.080 (0.073-0.095)	0.075 (0.052-0.094)	0.075 (0.058-0.085)	0.507	0.407	0.984	0.260
Angle velocity (rad/s)							
X-axis	0.032 (0.027-0.040)	0.031 (0.028-0.040)	0.035 (0.028-0.040)	0.775	0.590	0.514	0.984
Y-axis	0.053 (0.041-0.064)	0.041 (0.038-0.054)	0.037 (0.035-0.052)	0.087	0.199	0.333	0.034
Z-axis	0.039 (0.034-0.050)	0.033 (0.028-0.042)	0.033 (0.028-0.040)	0.243	0.199	0.737	0.128
Angle acceleration (rad/s²)							
X-axis	0.093 (0.087-0.132)	0.099 (0.083-0.127)	0.109 (0.090-0.124)	0.848	0.619	0.678	0.859
Y-axis	0.142 (0.129-0.188)	0.127 (0.118-0.145)	0.117 (0.107-0.175)	0.127	0.097	0.649	0.079
Z-axis	0.114 (0.098-0.131)	0.104 (0.082-0.113)	0.099 (0.083-0.115)	0.389	0.263	0.921	0.228
Angle Jerk (rad/s³)							
X-axis	0.288 (0.269-0.410)	0.302 (0.251-0.391)	0.332 (0.275-0.378)	0.821	0.590	0.621	0.921
Y-axis	0.439 (0.391-0.573)	0.391 (0.356-0.446)	0.358 (0.328-0.539)	0.109	0.106	0.707	0.055
Z-axis	0.351 (0.306-0.392)	0.319 (0.253-0.350)	0.301 (0.248-0.351)	0.339	0.245	0.921	0.185

Table S6. The motion metrics that contributed to the 1st, 2nd, and 3rd principal component in the PCA among the groups.

First principal component		Second principal component		Third principal component	
Motion metrics	Loading	Motion metrics	Loading	Motion metrics	Loading
Angular jerk of the straight forceps in the pitch axis	0.964	Acceleration of the straight forceps in the z-axis	0.767	Velocity of the pediatric backbiter forceps in the z-axis	0.672
Angular acceleration of the straight forceps in the pitch axis	0.959	Jerk of the straight forceps in the x-axis	0.751	Path length of the pediatric backbiter forceps in the x-axis	0.662
Angular jerk of the straight forceps in the yaw axis	0.952	Acceleration of the straight forceps in the y-axis	0.747	Path length of the pediatric backbiter forceps in the y-axis	0.657
Angular acceleration of the straight forceps in the yaw axis	0.940	Jerk of the straight forceps in the z-axis	0.742	Path length of the pediatric backbiter forceps in the z-axis	0.647
Acceleration of the upper forceps in the z-axis	0.822	Acceleration of the straight forceps in the x-axis	0.739		
Angular velocity of the upper forceps in the pitch axis	0.821				
Angular acceleration of the upper forceps in the pitch axis	0.816				
Angular jerk of the upper forceps in the pitch axis	0.811				
Jerk of the upper forceps in the z-axis	0.800				

Table S7. Motion metrics showing significant changes after the repetitive trainings.

Motion metrics	1st training	Final training	P value
Path length of pediatric back-biter forceps in the x-axis	0.792 (0.291-1.206)	0.334 (0.202-0.428)	0.049
Path length of pediatric back-biter forceps in the y-axis	1.090 (0.407-1.821)	0.380 (0.277-0.546)	0.027
Path length of pediatric back-biter forceps in the z-axis	0.986 (0.359-1.587)	0.372 (0.278-0.495)	0.027
Angular velocity of the straight forceps in the yaw axis	0.106 (0.089-0.124)	0.128 (0.116-0.157)	0.031
Angular velocity of the upper forceps in the forceps-in the pitch axis	0.102 (0.083-0.120)	0.123 (0.103-0.134)	0.027
Angular acceleration of the upper forceps in the pitch axis	0.302 (0.277-0.426)	0.442 (0.376-0.497)	0.004
Angular jerk of the upper forceps in the pitch axis	0.951 (0.86-1.325)	1.382 (1.14-1.557)	0.004

Table S8. The motion metrics measured in the repetitive training that contributed to the first and second principal components in the PCA.

First principal component		Second principal component	
Motion metrics	Loading	Motion metrics	Loading
Angular velocity of the straight forceps in the yaw axis	0.932	Path length of pediatric back-biter forceps in the z-axis	0.819
Angular acceleration of the upper forceps in the pitch axis	0.903	Path length of pediatric back-biter forceps in the x-axis	0.804
Angular jerk of the upper forceps in the pitch axis	0.903	Path length of pediatric back-biter forceps in the y-axis	0.797
Angular velocity of the upper forceps in the forceps-in the pitch axis	0.897		